Estimation of Multi-Constellation GNSS Observation Stochastic Properties Using a Single-Receiver Single-Satellite Data Validation Method

A. El-Mowafy

Department of Spatial Sciences, Curtin University, Australia
Email: a.el-mowafy@curtin.edu.au

ABSTRACT

The single-receiver single-satellite validation method is a technique that screens data from each satellite independently to detect and identify faulty observations. A new method for estimation of the stochastic properties of multi-constellation GNSS observation is presented utilizing parameters of this validation method. Agreement of the characteristics of the validation statistics with theory is used as the criterion to select the best precision of the observations, spectral density and correlation time of the unknowns. A curve fitting approach in an iterative scheme is employed. The method is applicable to any GNSS with any arbitrary number of frequencies. Demonstration of the method results and performance is given using multiple-frequency data from GPS, GLONASS and Galileo in static and kinematic modes.

KEYWORDS: Data Validation. GNSS. Observation Precision. Stochastic Properties.

INTRODUCTION

The knowledge of realistic values of observation precision is essential in building a reliable covariance matrix of the observations and in their weighting during processing in all precise positioning and navigation applications using Global Navigation Satellite Systems (GNSS). Estimation of the observation stochastic properties has been discussed in [1], [7], [15], [17], [22] and [26] mainly for conventional observations. With new measurements from emerging constellations of GNSS, estimation of observation precision for all constellations and for all their frequencies is needed. On the other hand, methods that are capable of validating data from multiple GNSS constellations should be implemented to detect extreme irregularities in the data and isolate faulty observations. [23, 24] evaluate a general form of fault detection and exclusion and discuss probabilities of different types of errors. Validation of GPS with GLONASS measurements was investigated in [6], and GPS with Galileo in [11] and [17].

The single-receiver single-satellite approach is a method that can be applied to validate any GNSS with any arbitrary number of frequencies. The basic model of the method was discussed in [4] and [19], and was presented in a modified form in [10]. In this contribution, the single-receiver single-satellite data validation method is firstly reviewed as a background to the main focus of this paper, which is presenting a new method for estimation of the stochastic properties of the multi-constellation observations by examining statistical properties of the validation statistics. Agreement of the characteristics of the validation statistics with theory is used as the criterion to select the best precision of the observations within an iterative search process. Such agreement will take place when real-data are correctly modelled and their assumed stochastic properties are properly selected. Demonstration of the proposed method is given in static and kinematic modes. The static test include observations collected over one week at two continuously operating reference

stations, and the kinematic data were collected in a ship-borne mode for nine hours. The paper presents estimation of precision and stochastic properties of current observation types from the three GNSS: GPS, GLONASS and Galileo.

SINGLE-RECEIVER SINGLE-SATELLITE DATA VALIDATION METHOD

In the single-receiver single-satellite method, undifferenced code and phase observations of each satellite of a single receiver are screened to detect the most severe irregularities in the data and if necessary remove or repair faulty observations. The process is applied, satellite by satellite, independently at each epoch, and in a sequential manner. The method is applicable to post-mission or real-time processing of any GNSS constellation, in static or kinematic modes. In addition, the method advantages include that measurements from systems with a limited number of operational satellites, such as Galileo and QZSS, can be screened without the need for having a complete positioning solution. Moreover, there is no need for the determination of inter-system biases when using data from different constellations as the model does not combine data from different systems, where observations from each satellite are screened individually. In this section, the mathematical modelling used in the method in addition to the validation process employed are presented.

A Reparameterized Modelling Form of the Observation Equations

The carrier phase and pseudorange observation equations of a single satellite tracked by a single receiver on frequency f_j (for j = 1 to n) at time instant t can be formulated as follows:

$$\phi_j(t) = \rho(t) + d\rho(t) + c\big(\delta t_r(t) - \delta t^s(t)\big) + T(t) - \mu_j I(t) + b_{\phi_j}(t) + \tilde{b}_{\phi_j}(t) + \varepsilon_{\phi_j}(t) \quad (1)$$

$$p_j(t) = \rho(t) + d\rho(t) + c\big(\delta t_r(t) - \delta t^s(t)\big) + T(t) + \mu_j I(t) + b_{p_j}(t) + \tilde{b}_{p_j}(t) + \varepsilon_{p_j}(t) \quad (2)$$

where $\phi_j(t)$ and $p_j(t)$ denote the observed carrier phase and pseudoranges in distance units with corresponding zero-mean noise terms $\varepsilon_{\phi_j}(t)$ and $\varepsilon_{p_j}(t)$. $\rho(t)$ denotes the receiver-to-satellite range, $d\rho(t)$ is the orbital error, c is the speed of light, $\delta t_r(t)$ and $\delta t^s(t)$ are the receiver and satellite clock errors and $T(t)$ is the tropospheric delay. The parameter $I(t)$ denotes the ionospheric delay for code observations and advance for phase observations expressed in units of distance with respect to the first frequency. For frequency f_j, the ionospheric coefficient $\mu_j = f_1^2/f_j^2$ is used to express the ionosphere error in terms of $I(t)$. The parameters $b_{\phi_j}(t)$ and $b_{p_j}(t)$ are the phase and code biases, which are considered constant over a short period of time [**8**, **19**], e.g. an hour, and therefore will be denoted thereafter as $b_{\phi_j}(t_o)$ and $b_{p_j}(t_o)$. For phase measurements, $b_{\phi_j}(t_o)$ comprises the sum of the initial phase bias, the phase ambiguity and the instrumental phase delay. For code measurements, $b_{p_j}(t_o)$ is the instrumental code delay. $\tilde{b}_{\phi_j}(t)$ and $\tilde{b}_{p_j}(t)$ denote the unmodelled systematic errors that are not constant in nature or quasi-random, such as multipath.

The ionospheric delay $I(t)$ and the bias parameters $\tilde{b}_{\phi_j}(t)$ and $\tilde{b}_{p_j}(t)$ can be split into two components, initial values $I(t_o)$, $\tilde{b}_{\phi_j}(t_o)$ and $\tilde{b}_{p_j}(t_o)$ at the initial epoch t_o, and the difference from these value, which are denoted as $\delta I(t)$, $\delta \tilde{b}_{\phi(t)}$ and $\delta \tilde{b}_p(t)$ such that:

$$I(t) = I(t_o) + \delta I(t) \quad\quad\quad\quad (3)$$

$$\tilde{b}_{\phi_j}(t) = \tilde{b}_{\phi_j}(t_o) + \delta\tilde{b}_{\phi_j}(t) \tag{4}$$
$$\tilde{b}_{p_j}(t) = \tilde{b}_{p_j}(t_o) + \delta\tilde{b}_{p_j}(t) \tag{5}$$

The rank deficiency of the model in Eq. (1, 2) can be reduced by re-parameterization of the unknowns using a geometry-free model as follows [10]:

$$\rho^*(t) = \rho(t) + d\rho(t) + c(\delta t_r(t) - \delta t^s(t)) + T(t) \tag{6}$$
$$\rho^{**}(t) = \rho^*(t) - \rho^*(t_o) \tag{7}$$
$$b_{\phi_j}^*(t_o) = b_{\phi_j}(t_o) + \tilde{b}_{\phi_j}(t_o) + [\rho^*(t_o) - \mu_j I(t_o)] \tag{8}$$
$$b_{p_j}^*(t_o) = b_{p_j}(t_o) + \tilde{b}_{p_j}(t_o) + [\rho^*(t_o) + \mu_j I(t_o)] \tag{9}$$

The observation equations in terms of the re-parameterized vector of unknowns $[\rho^{**}(t), \delta I(t), b_{\phi_j}^*(t_o), b_{p_j}^*(t_o), \delta\tilde{b}_{\phi_j}(t), \delta\tilde{b}_{p_j}(t)]^T$ then read:

$$\phi_j(t) = \rho^{**}(t) - \mu_j \delta I(t) + \delta\tilde{b}_{\phi_j}(t) + b_{\phi_j}^*(t_o) + \varepsilon_{\phi_j}(t) \tag{10}$$
$$p_j(t) = \rho^{**}(t) + \mu_j \delta I(t) + \delta\tilde{b}_{p_j}(t) + b_{p_j}^*(t_o) + \varepsilon_{p_j}(t) \tag{11}$$

During processing initialization, the first three terms on the right-hand side of the equation equal zeros at the first epoch t_o, leading to $b_{\phi_j}^*(t_o)$ and $b_{p_j}^*(t_o)$ equal $\phi_j(t_o)$ and $p_j(t_o)$, respectively. The unknowns in Eq. (10, 11) can be predicted using dynamic modelling to remove rank deficiency in a Kalman filtering processing. The time prediction process at time t for the vector of unknowns, denoted in a general form as x_t, reads:

$$\check{x}_t = \Phi_{t/t-1}\hat{x}_{t-1} \tag{12}$$

where $\Phi_{t/t-1}$ is the transition matrix, $\hat{x}_{t-1}$ and $\check{x}_t$ are the estimated and predicted vectors of unknowns at times t-1 and t. The reparametrized unknown range ρ^{**} can be considered unlinked in time and thus is not considered in the prediction process. $b_{\phi_j}^*(t_o)$ and $b_{p_j}^*(t_o)$ are constants. The ionospheric delay δI and the time-variant bias components $\delta\tilde{b}_{\phi_j}$ and $\delta\tilde{b}_{p_j}$ are considered changing relatively smoothly with time and taken exponentially decaying by using a first-order autoregressive stochastic process (a first-order Gauss-Markov process). Hence, the temporal correlations of the biases, denoted in a general term as β reads:

$$\beta = e^{-|\Delta t|/\tau} \tag{13}$$

where e is the base of the natural logarithm, Δt is the time interval between the epochs $t - 1$ and t and τ is the correlation time length. The dynamic models of δI, $b_{\phi_j}^*$ and $b_{p_j}^*$ for a frequency j at t then read:

$$\delta I(t) = \beta_{\delta I}\, \delta I(t - 1) + d_{\delta I}(t) \tag{14}$$
$$b_{\phi_j}^*(t) = \beta_{b_{\phi_j}^*}\, b_{\phi_j}^*(t - 1) + d_{b_{\phi_j}^*}(t) \tag{15}$$
$$b_{p_j}^*(t) = \beta_{b_{p_j}^*}\, b_{p_j}^*(t - 1) + d_{b_{p_j}^*}(t) \tag{16}$$

where $\beta_{\delta I}$, $\beta_{b_{\phi_j}^*}$ and $\beta_{b_{p_j}^*}$ are the temporal correlations for $\delta I(t)$, $b_{\phi_j}^*(t)$ and $b_{p_j}^*(t)$. $d_{\delta I}(t)$, $d_{b_{\phi_j}^*}(t)$ and $d_{b_{p_j}^*}(t)$ are their process noises, which are assumed Gaussian white noises. The variance of each process noise is computed as $\{\frac{\vartheta}{\frac{2}{\tau}}(1-\beta^2)\}$ [13], where ϑ denotes the spectral density. The transition matrix $\Phi_{t/t-1}$ is taken a digonal matrix comprising the temporal correlations $\beta_{\delta I}$, $\beta_{b_{\phi_j}^*}$ and $\beta_{b_{p_j}^*}$.

Data Validation Process

For validation of GNSS data, one starts by formulation of the observation equation at time *t* in a linearized Gauss–Markov model as follows:

$$y_t = A_t \breve{x}_t + \hat{v}_t \tag{17}$$

where y_t is the vector of phase and code observations, $\hat{v}_t$ denotes the vector of observation predicted residuals (innovations) and A_t is the design matrix, which reads:

$$A_t = \begin{bmatrix} u & -\mu_j & I & 0 & I & 0 \\ u & +\mu_j & 0 & I & 0 & I \end{bmatrix} \tag{18}$$

for *j*=1 to *n* frequencies, *u* is a unit column vector and I is the identity matrix, both of size *n*.

In real-time applications, *Local Testing* can be applied, where one examines the observations at the present epoch. *q* number of possible errors in the observations can be tested, where *q* < *df*, where *df* is the degrees of freedom. Possible detection of the presence of model errors can be performed by examining the local over-all model statistic T_{LOM}, which reads [20]:

$$T_{LOM} = \hat{v}_t^T Q_{\hat{v}_t}^{-1} \hat{v}_t / df \tag{19}$$

where $Q_{\hat{v}_t}$ denotes the covariance matrix of the predicted residuals, formulated as [20]:

$$Q_{\hat{v}_t} = Q_{y_t} + [A_t(A_t^T Q_{y_t}^{-1} A_t)^{-1} A_t^T] \tag{20}$$

Q_{y_t} is the covariance matrix of the observations. The null hypothesis (outlier-free observations) is rejected, indicating possible presence of significant measurement or model errors, when:

$$T_{LOM} \geq F_\propto(df, \infty, 0) \tag{21}$$

where $F_\propto$ is the Fisher distribution value corresponding to a significance level α and *df*.

Once the presence of an observation outlier is detected, one needs to identify the faulty measurement(s) that cause such error(s). We will restrict attention to one dimensional error model in one code or phase observation, i.e. $q = 1$. The test statistic can then be computed for observation *i* as follows [2, 20]:

$$w_i = \frac{c_i^T \, Q_v^{-1} \, \hat{v}}{\sqrt{(c_i^T \, Q_{\hat{v}} \, c_i)}} \tag{22}$$

where c_i is a zero column vector except the element corresponding to the examined observation i, which equals 1. An outlier is considered present in the observation when:

$$|w_i| \ge N_{\frac{\alpha 1}{2}}(0,1), \quad |w_i| \ge |w_k| \quad \text{for } k= 1 \text{ to } m \text{ observations} \tag{23}$$

Note that the significance level $\alpha 1$ for the w-statistic is different from the significance level α for the local over-all-model in the detection test. The former can be computed using Baarda's B method [1], which assumes same probability for type II error (failure to reject a false null hypothesis) in both the detection and identification tests.

The power of the above test statistic can be assessed by its Minimal Detectable Biases (*MDB*), which is a measure for the size of the error that can be detected with a certain power and probability of false alarm. The *MDB* reads [4, 20]:

$$MDB_i = \sqrt{\frac{\lambda_o}{(c_i^T \, Q_{\hat{v}} \, c_i)}} \tag{24}$$

The non-centrally parameter λ_o needs first to be determined, where [20]:

$$\lambda_o = f(\alpha, \gamma, q) \tag{25}$$

γ denotes the power of the test. The *MDB* can be computed even before actual measurements have been collected using only the functional model and the expected precision of the data.

UTILIZATION OF THE PROPERTIES OF w-STATISTIC AS A TOOL TO ESTIMATE OBSERVATION STOCHASTIC PROPERTIES

This section discusses the characteristics of the validation parameters of the single-receiver single-satellite approach that can be used as a tool for estimation of the observation stochastic properties. For instance, one can check that the estimated w-statistic of the observed signals has a standard normal distribution, N(0, 1). Such a condition would only take place if observation weighting is correctly applied under the null hypothesis. A demonstration of the proposed approach is given through implementation in practical experiments in the static and kinematic modes. Due to the large number of figures that can be discussed in this demonstration, only representative samples are presented.

Test Description

The data used in the static test were collected at two continuously operating reference stations at Curtin University, Australia, over the first week of March 2013 with 30 seconds sampling interval. Observations from GPS, GLONASS and Galileo were collected using a geodetic-grade multi-frequency multi-GNSS antenna (TRM59800.00) and receiver (Trimble NETR9). Tracked signals in the test included L1, L2 and L5 code and phase observations for GPS, L1 and L2 for GLONASS, and E1, E5a and E5b for Galileo.

The kinematic test was carried out on 26/4/2012, where the GNSS was mounted on a boat and almost 9.3 hours of GPS and GLONASS data with a sampling interval of one second were collected using a Sokkia GSR2700ISX receiver. The kinematic course included a high dynamic part where the boat was almost six kilometres offshore

Characterization of w-test statistic As a Tool to Estimate Observation Precision

Figures 1 to 3 show three examples from processing the static data of GPS satellite PRN 29, GLONASS PRN 19 and Galileo PRN 11 collected on 2/3/2013 using the single-receiver single-satellite data validation method. The figures depict the time-series and histograms of w-statistic for phase and code data of all available frequencies with the elevation angle and signal-to-noise ratio (SNR) values in dB-Hz for L1. The elevation angles were obtained from satellite almanacs and approximate point positions determined using a single point positioning of available GPS data performed in a prior step to the data screening process. The left side of the Figures 1 to 3 shows time-series of the computed w- statistic values and the right side of the figures shows their corresponding histograms, where the computed standard deviation σ_w and mean μ_w of each w-statistic are given on top of each figure. Figure 4 illustrates a similar example for the kinematic test, where the w-statistic values for GPS PRN 31 is given as an example. The similarities shown in the between w-statistic values for ϕ_1 and ϕ_2 in the four figures can be explained by their correlations, which results in an error in one measurement influencing other measurements [**14**]. The critical values for w-statistic $[N_{\frac{\alpha}{2}}(0,1)]$ are shown in the figures as solid lines. A possible outlier is suspected when the computed w-statistic exceeds this critical value.
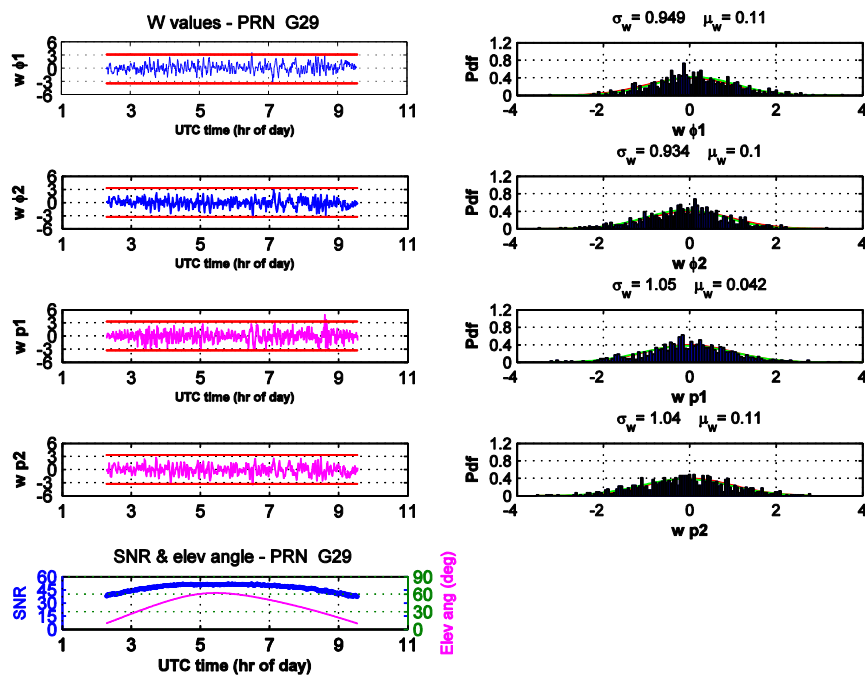

Fig. 1. Time-series of w-statistic for GPS phase and code measurements on L1 and L2, satellite elevation angles and SNR on L1 (left side); histograms of w-statistic (Right side)
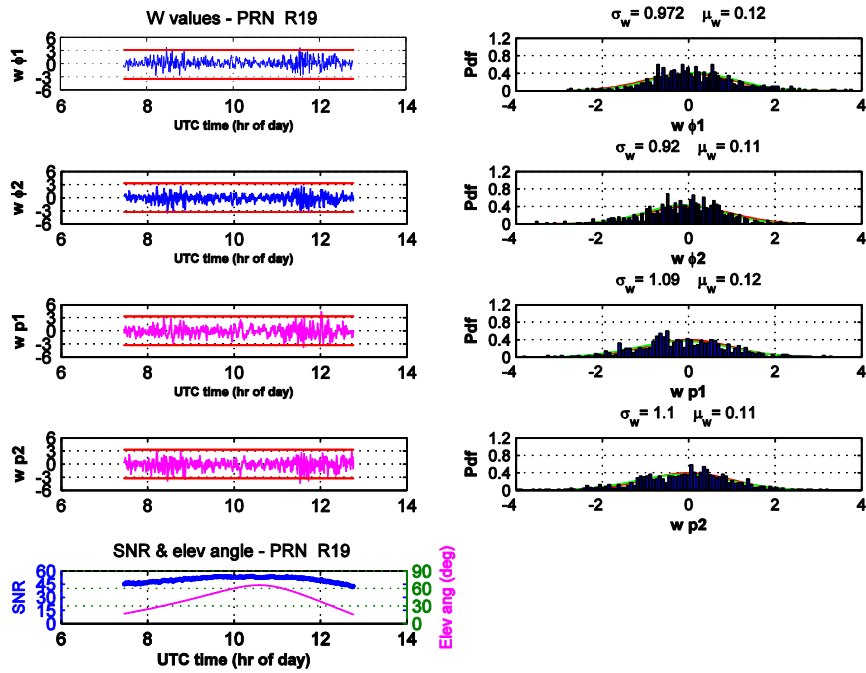
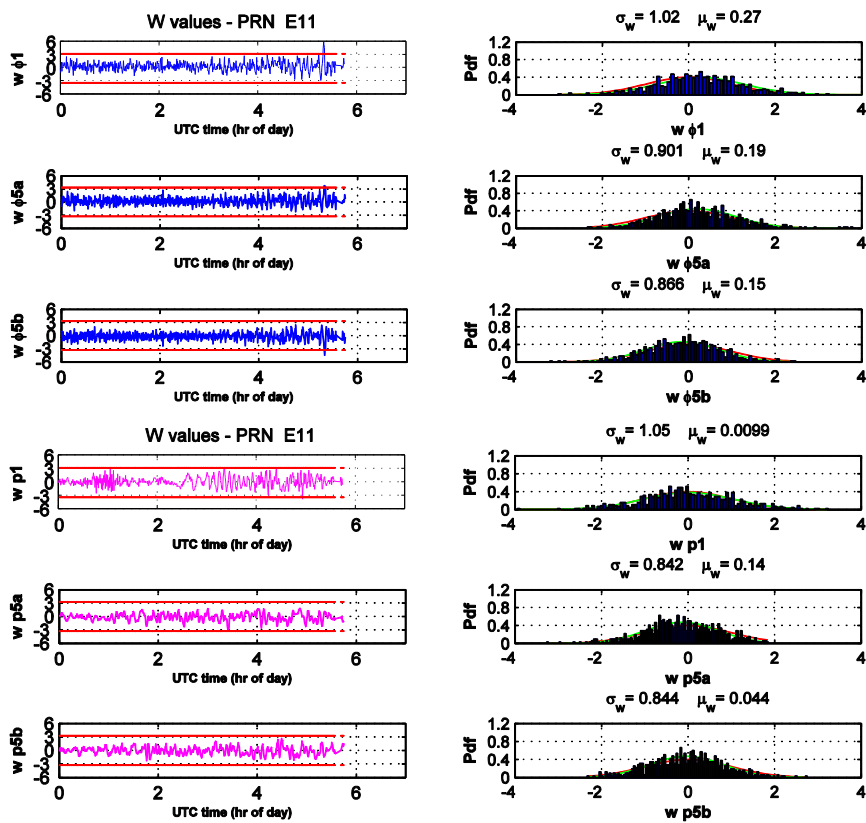Fig. 2. Time-series and histograms of w-statistic for GLONASS measurements

Fig. 3. Time-series and histograms of w-statistic for Galileo measurements
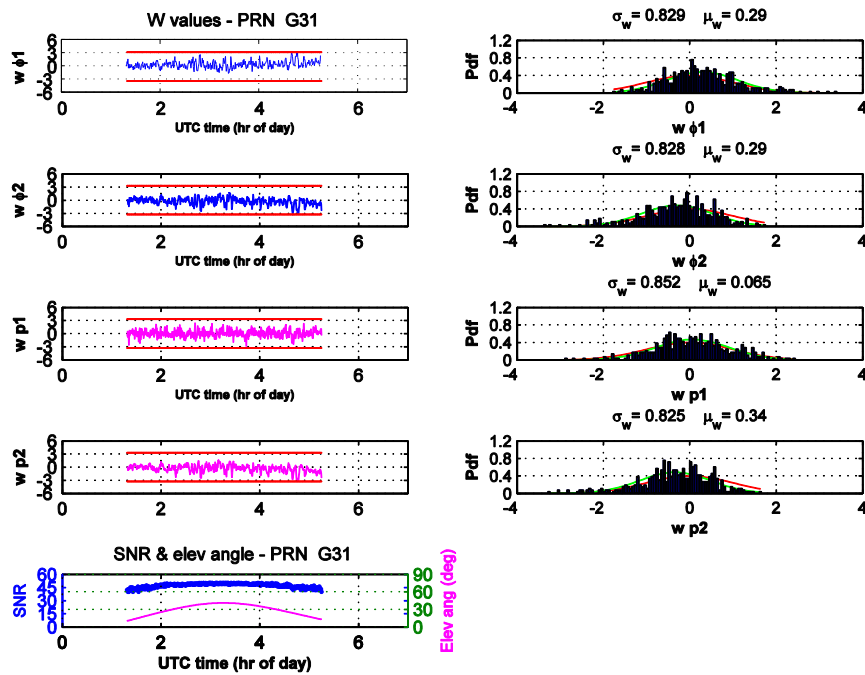
Fig. 4. Time series of w-statistic in the kinematic test

To check if the w-statistic approximately follows a standard normal distribution, a number of methods can be applied. For instance, one would consider the closeness of the standard deviations to one and the mean values to zero. Ideally this would be the case, however, due to possible noise in the data, small discrepancies may be experienced. In addition, one can judge by visual inspection of the w-statistic histograms to check if they vary in a random manner, with a standard normal distribution. This is shown in the Figures 1 to 4, for which the model and stochastic information are set correctly. On the other hand, Figure 5 illustrates a case where the process noise parameters were incorrectly set (amplifying the C/A code standard deviations by 10 times of the assumed correct value) for GPS satellite PRN 29. As shown in Figure 5, the w-statistic histograms significantly deviate from the standard normal distribution. An alternative method is to inspect the Q-Q plot of the w-statistic, where a departure of the data from the Q-Q slant straight line would indicate departure from normality. An example of a Q-Q plot for GPS w-statistic results of C/A code data for satellite PRN 29 is given in Figure 6. A skewness or short/long tails of points on a Q-Q plot would indicate skewness and tailing of data distribution. Inference of the plot would help in tuning the variance of the observations. For instance, long tails with an 'S' shaped-curve indicates that the data have more variance than expected from data of a normal distribution. This is shown in Figure 7 for the case of amplifying the C/A code standard deviations of GPS satellite PRN 29. On the other hand, short tails indicate less variance than one would expect. Finally, the Kolmogorov-Smirnov goodness-of-fit test [16] can be performed which compares the cumulative distribution function (CDF) of the time-series of the w-statistic to the hypothesized CDF of continuous distribution defined by the standard normal distribution.
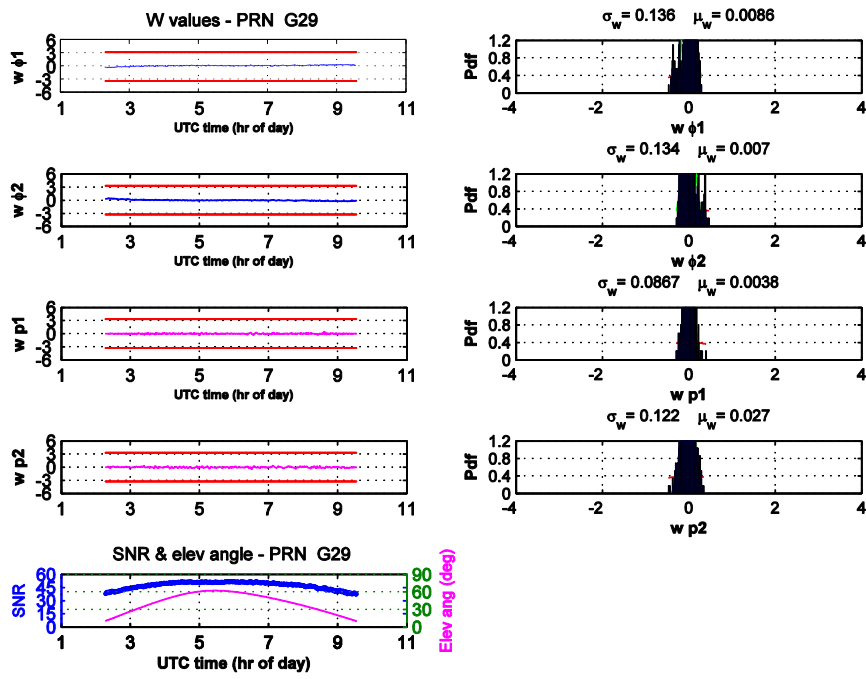
Fig. 5. w-test statistic for measurements with incorrect process noise modelling
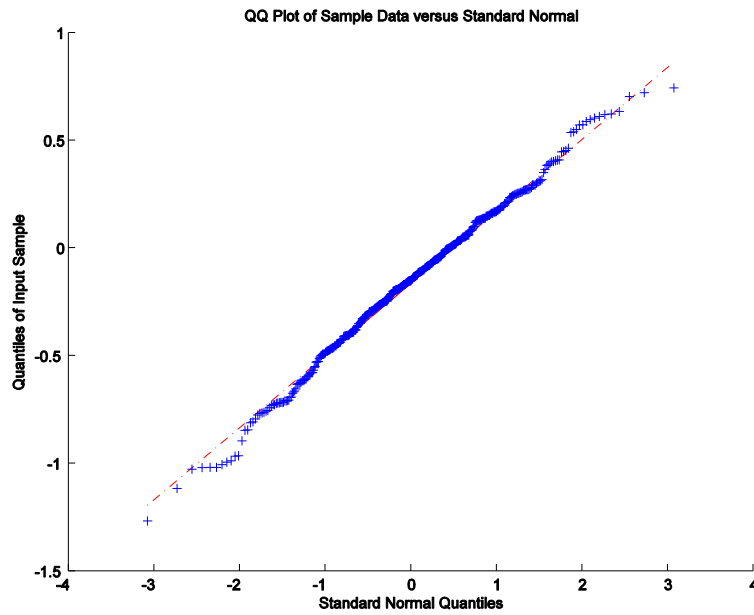

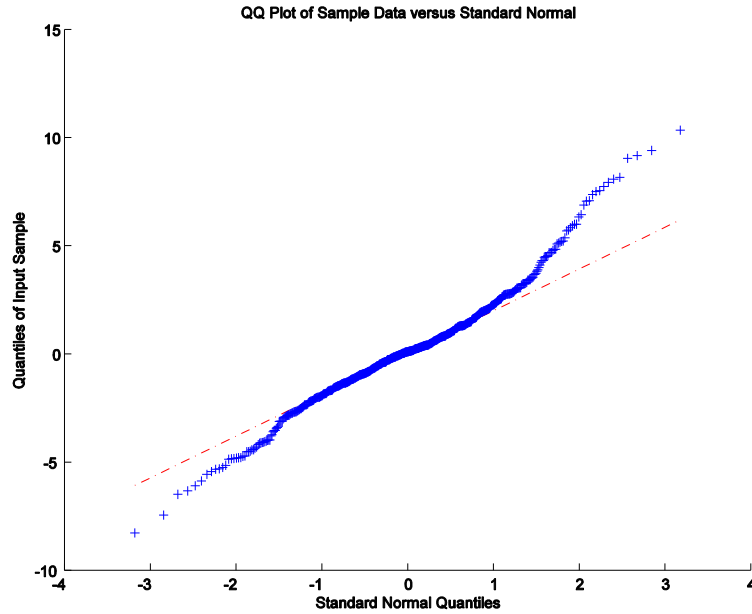Fig. 6. Q-Q plot for GPS C/A code data of satellite 29

Fig. 7. Q-Q plot for GPS C/A code data of satellite 29 with a wrong standard deviation

ESTIMATION OF STOCHASTIC PROPERTIES OF THE MULTI-GNSS OBSERVATIONS
AND PROCESS NOISE

A new empirical method for estimation of the stochastic properties of the observations and the process noise using the validation parameters of the single-receiver single-satellite technique is described in this section. While the precision of conventional observations of GPS and GLONASS has been researched before, the method is of particular interest for the modernized observation types of the two systems and for the new GNSS constellations. Results for different types of phase and code observations of currently available frequencies in each of the tested constellations: GPS, GLONASS and Galileo are presented using real data.

The performance of the multi-frequency multi-constellation single-satellite validation method is affected by the covariance matrix of the observations. To compute the standard deviations used in the covariance matrix for the slant observations along the receiver-to-satellite line of sight used in computing the covariance matrix, two methods were considered in this study. In the first method, the standard deviations along the slant directions were computed by scaling the standard deviations along the zenith using an elevation-angle dependent model in the form $[1 + a_0 \times exp(-E^o/E_o^o)]$ [12], where a_0 is a weighting coefficient that is dependent on the type and frequency of the observation, receiver and method used for the observation tracking (e.g. Z-tracking, codeless, semi-codeless). E^o and E_o^o are the observed elevation angle and a selected base value for the elevation angle in degrees. In this study, the weight model is selected as $(1 + 10 \times e^{(-E^o/10^o)})$ with an average value of $a_0 = 10$, such that for observation i, its variance reads [21]:

$$\sigma_i^2 = \sigma_o^2(1 + 10 \times e^{(-E^o/10^o)})^2 \tag{26}$$

where σ_o^2 is the variance along the zenith direction. The second weight model considered employs the Carrier-to-Noise density ratio (or the signal-to-noise ratio, *SNR*) in the form [27]:

$$\sigma_i^2 = Z_i \times 10^{-\frac{SNR_i}{10}} \tag{27}$$

where Z_i is a variance factor that is dependent on the type and frequency of the observation, the method used for observation tracking, and receiver used. SNR_i is the measured signal-to-noise ratio for the observation i in dB-Hz.

Estimation of the Precision of the Multi-GNSS Observations

In this approach, the tested un-differenced GNSS measurements were assumed with no cross-correlations. The standard deviations of the undifferenced observations along the zenith direction are empirically determined using a curve fitting iterative method. The data used were collected throughout the first week of March 2013 in the static mode, which is a controlled environment suitable for this purpose. Possible values of standard deviations were iteratively used in the validation process and the set that gave the best overall fit of the distribution of w-test statistic to N(0, 1) for most satellite observations of each system and passed all normality tests mentioned in the previous section was selected as the best candidate.

Standard deviations of the phase observations were iterated within the range 0.5 mm to 3 mm for all GNSS systems. For code observations, standard deviations of GPS and Galileo measurements were examined between 5 cm and 25 cm. For GLONASS code observations, the range of iterated standard deviations was from 5 cm to 40 cm, due to the fact that GLONASS observations typically have less precision compared with the observations of GPS and Galileo. Using an elevation-angle dependent model (Eq. 26), testing was performed for each observation type, starting the standard deviation from a base value and incrementing it by 0.1 mm for phase observations and by 1 cm for code observations. The best obtained sets of standard deviations for the three GNSS are given in Table 1, noting that most multipath effects were modelled in the terms $\delta\widetilde{b}_{\phi_j}$ **and** $\delta\widetilde{b}_{p_j}$. The presented values are in close agreement with the measurement precision given in the literature [5, 23].

Table 1. Standard deviations of undifferenced GNSS measurements (zenith direction)

	GPS			Galileo				GLONASS	
	L1	L2	L5	E1	E5a	E5b	E6	L1	L2
code (cm)	20	10	5	20	12	11	5	33	20
phase (mm)	1.5	1.3	1.0	2.0	0.6	0.6	0.7	2.2	2.0

The second weight model considered in this study employs the signal-to-noise ratio (*SNR*). The variance factor in this model was estimated by considering the zenith direction, where *SNR* usually reach their maximum values. By substituting the variance of the observations on the left-hand side of Eq. (27) to the estimated values along the zenith direction listed in Table 1 and using the maximum possible values for *SNR* of different observation types obtained from the used receiver, one can estimate Z_i. In this study, the maximum values of *SNR* for different observation and frequency types ranged between 47.9 and 56.7 dB-Hz.

The competency of the two methods, elevation-angle and SNR-dependent modelling, in weighting of the observations in the validation method is presented here through one example by comparing Figure 1 with Figure 8 for GPS observations of satellite PRN 29. The later figure illustrates the distribution of w-statistic values based on using the SNR weighting model, whereas Figure 1 is based on weighting the observations using the elevation-angle

dependent model. As the two figures show, the standard deviations σ_w and the mean μ_w of the w-statistic results of the two methods almost agree with minor differences. This result comes to an agreement with other studies that compare the impact of using the two methods on positioning performance [**3**].
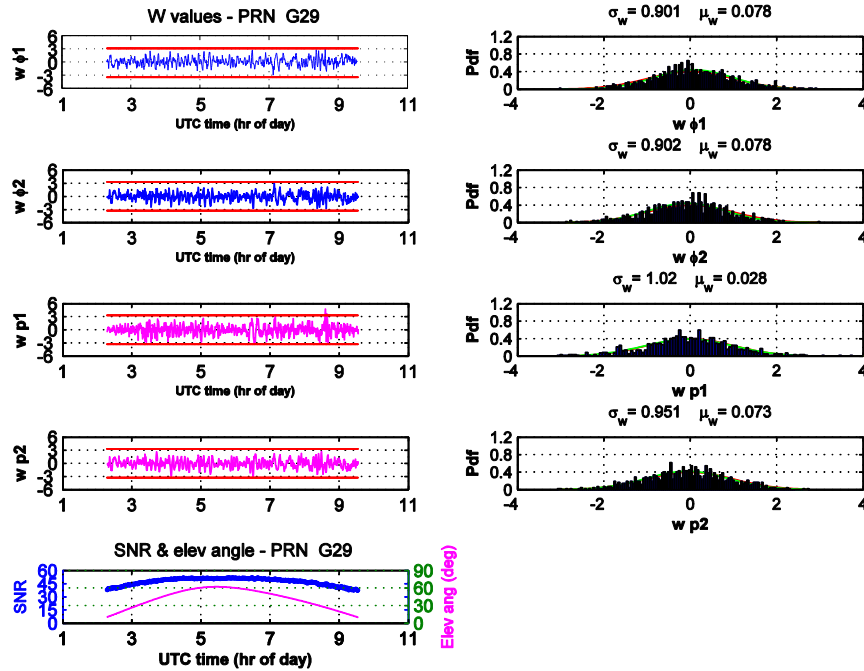

Fig. 8. Time series and histogram of w-test statistic for GPS weighting using SNR

Estimation of Correlation times and Spectral Densities

In addition to the covariance matrix of the observations, stochastic information needed for processing using the single-receiver single-satellite validation method include the process noise of the unknowns δI, $\delta \widetilde{b}_{\phi_j}$ and $\delta \widetilde{b}_{p_j}$. Since these unknowns are modelled as a first-order Gauss-Markov process with a correlation that is decaying exponentially with time, their correlation times were determined by plotting the autocorrelation of each element as a function of time lag and estimating the time lag at which the autocorrelation equals $1/e$. The correlation time for $\delta I, \delta \widetilde{b}_{\phi_j}$ and $\delta \widetilde{b}_{p_j}$ are given in Table 2 for the static test data based on processing results of the first week of March 2013. To determine the best values for the spectral densities ϑ, they were initially taken as the change of the parameters with time. Next, these values were tuned utilizing the same approach used in estimating the precision of the observations, i.e. selecting the set that gives the best overall fit of the distribution of w-statistic values to N(0, 1) and passes all normality tests. The best estimated spectral densities under our test conditions are given in Table 2. These values were considered applicable for all frequencies and for all GNSS systems as our tests show.

Table 2. Spectral densities of the process noise of the model parameters in the static mode

Parameter	δI	$\delta \widetilde{b}_{\phi}$	$\delta \widetilde{b}_{p}$
Spectral densities	$4\ mm^2/s$	$1.5\ mm^2/s$	$47\ mm^2/s$
Correlation time	600 s	600 s	600 s

For the kinematic test data, the observation precisions determined in the static mode were used; however, the spectral densities have to accommodate possible changes due to dynamics of the object and surrounding environment. Keeping the same correlation time of the time-variant biases for both the static and kinematic modes, the same strategy discussed in the static mode for estimation of the best values for the spectral densities ϑ was followed. The spectral densities were initially taken as the estimated values in the static mode and were next tuned to find the set that gives the best overall fit of the distribution of w-statistic to normal distribution under our test conditions after excluding data outliers. In the ship-borne kinematic environment considered here, the boat has experienced relatively medium waves. As a result, the spectral densities in the kinematic mode were slightly higher than those for the static test. The final spectral densities for the kinematic test are given in table 3.

Table 3. Spectral densities of the process noise of in the Kinematic mode

Parameter	δI	$\delta \tilde{b}_\phi$	$\delta \tilde{b}_p$
Spectral densities	$4 \, mm^2/s$	$2 \, mm^2/s$	$60 \, mm^2/s$
Correlation time	600 s	600 s	600 s

Testing the Estimated Stochastic Properties of GNSS Observations

After estimation of the stochastic properties of GNSS measurements, one would like to examine if they would produce realistic positioning results. Therefore, the estimated observation precisions of GPS were implemented in a Precise Point Positioning (PPP) processing of the ship-borne kinematic data. Note here that the GNSS observation precisions were obtained from the static data, i.e. they were independent from the data used in PPP processing. The single-receiver single-satellite data validation method was also used for screening the data prior to applying the PPP. A detection and exclusion strategy was applied, i.e. if an outlier is detected in any observation, this observation is excluded from the data.

Before using the validation approach, one would first examine its power through estimating the *MDB* values, which is a measure of the size of the errors that can be detected with the model used with a certain power of detection and probability of false alarm. Using 0.001 for the latter and a power of detection of 0.8, which are reasonable values for precise positioning, the resulting *MDBs* for GPS satellite 31, given as an example, are depicted in Figure 9. The figure shows that for high elevation angles, errors as low as 10 cm and less than a metre can be detected for GPS phase and code data respectively. However, for low elevation angles, the size of the minimum errors that can be detected significantly increases.
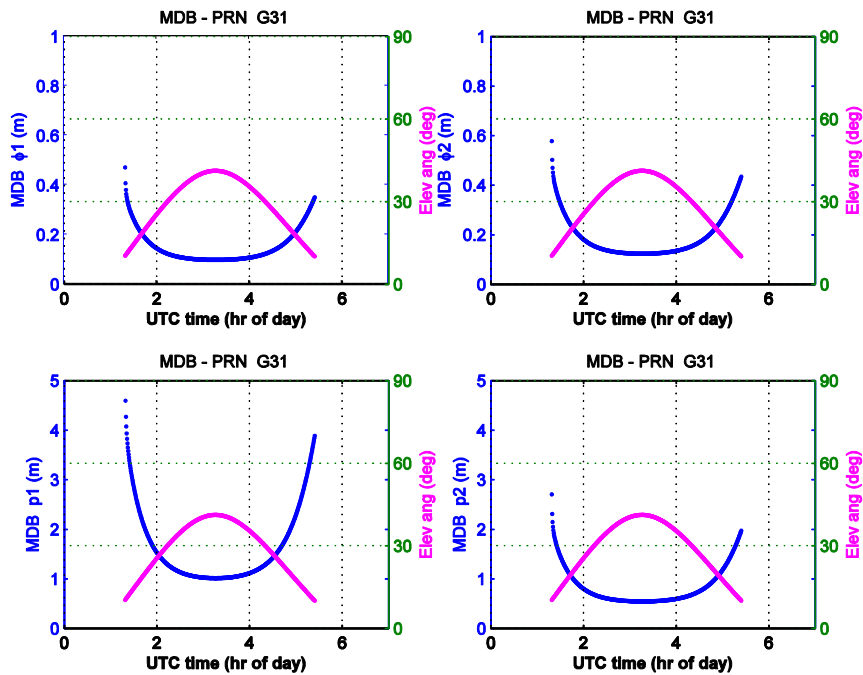
Fig. 9. MDB of GPS PRN 31

The time-series of the 3D position standard deviations, as a measure of position precision, resulting from processing the data in the PPP mode is given in Figure 10. As the figure shows, no outliers can be seen in the data after applying the single-receiver single-satellite validation method as outliers if present would result in spikes in the figure. This indicates the good performance of the single-receiver single-satellite validation method in detecting and removing observations with outliers if they exist. More results on the performance of the method in detection of different levels of artificially inserted outliers in a large data set are given in [10]. Furthermore, the resulting positions for the converged part of the solution were compared with the output of processing the data using the Natural Resources of Canada CSRS-PPP online service utilizing its default values [9]. The differences between the results of the two processing schemes were within a few mm to cm throughout the compared processing period, which indicated that the estimated observation precision used in the PPP processing were representative.
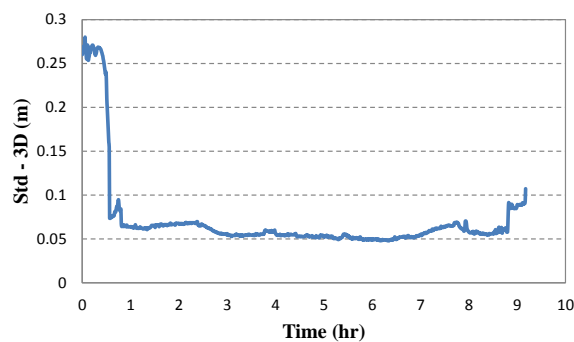

Fig. 10. 3D Positional Standard Deviation

CONCLUSIONS

A new empirical method for estimation of the precision of GNSS observations applicable to any GNSS with any number of frequencies is presented. While the precision of conventional observations of fully operational systems such as GPS and GLONASS has been identified before, the method is of particular interest for the new observation types of the modernized satellites and for the new GNSS constellations. The method uses the statistical properties of the single-receiver single-satellite local validation parameters to select the best precision of the observations applying a curve fitting iterative approach. The set that gives the best overall fit of the distribution of w-test statistic to a standard normal distribution for most satellite observations of each system and pass all normality tests is deemed suitable. In this study, real data from GPS, GLONASS and Galileo were used for this purpose. The data were collected throughout the first week of March, 2013 in a static mode, and for almost nine hours in a kinematic ship-borne mode. Values for the observation precision for different observation types of the three GNSS constellations were estimated and found to be in close agreement with their values determined from other studies. Two weighting models were considered, an elevation-angle dependent model and a model that uses Carrier-to-Noise density ratio. Results of the two methods were compatible. In addition, the spectral densities and correlation time of the unknowns were estimated for both static and kinematic test modes. In a practical positioning scenario, the single-receiver single-satellite validation method was firstly used for screening the kinematic boat data to detect outliers and identify erroneous observations. The measurement precisions that were estimated in the static testing were next used in PPP post-processing of the kinematic test data. Results showed the good performance of the single-receiver single-satellite data validation method in the detection of outliers and in removing faulty observations. The estimated observation precision from the presented tests gave comparable positioning solution to those obtained from a good independent source. However, as the method is empirical it requires long computation time for running possible candidate precisions within the chosen test range. In addition, the computed precisions do not include multipath; therefore, its impact should be accounted for in the processing schemes that merge its effect within the observation standard deviations. For the new systems, BeiDou, QZSS, IRNSS, we plan to conduct a future similar study to determine their stochastic properties.

ACKNOWLEDGMENT

References

1. Amiri-Simkooei A.R., Zangeneh-Nejad F., Asgari J., 2013. Least-squares variance component estimation applied to GPS geometry-based observation model. J Surv Eng. 139(4): 176-187
2. Baarda, W.A., 1968. *A testing procedure for use in geodetic networks*, Netherlands Geodetic Commission, Publications on Geodesy, New Series, **2**(5).
3. Collins, J.P., and Langely, R.B., 1999. Possible Weighting Schemes for GPS Carrier Phase Observations in the Presence of Multipath. *Technical Report Number 98151, Dept. of Geodesy and Geomatics Engineering, The University of New Brunswick, Canada*, 1-33.
4. De Bakker, P.F., Van der Marel, H., and Teunissen, P.J.G., 2009. The Minimal Detectable Bias for GNSS Observations with a Single Receiver Setup and a Geometry-Free Model. *Proceedings of ENC-GNSS 2009*, Naples, Italy, 3-6 May 2009.

5. De Bakker, P.F., Van der Marel, H., and Tiberius, C.C.J.M., 2009. Geometry-free undifferenced, single and double differenced analysis of single frequency GPS, EGNOS and GIOVE-A/B measurements. *GPS Solutions*, **13**(4): 305-314.

6. De Jong, K., Van der Marel, H., and Jonkman, N., 2001. Real-Time GPS and Glonass Integrity Monitoring and Reference Station Software. *Physics and Chemistry of the Earth (A),* **26**(6-8): 545-549.

7. El-Mowafy, A., and K.P. Schwarz, 1995. Epoch by Epoch Ambiguity Resolution for Real-Time Attitude Determination Using a GPS Multi-Antenna System. *Navigation, Journal of the US ION*, **42**(2), 391-408.

8. El-Mowafy, A., 2009. An Alternative Post-Processing Relative Positioning Approach Based on Precise Point Positioning. *J. of Surveying Engineering*, **135**(2): 56-65.

9. El-Mowafy, A., 2011. Analysis of the Web-Based Post-Processing GNSS Services for Static and Kinematic Positioning in Surveying Applications of Short Data Spans, *Survey Review*, **43**-323, 535-549.

10. El-Mowafy, A., 2014. GNSS Multi-frequency Receiver Single-Satellite Measurement Validation Method, *GPS Solutions*, Published online in Nov. 2013, DOI 10.1007/s10291-013-0352-6.

11. Ene, A., Blanch, J., and Powell, J.D., 2007. Fault Detection and Elimination for Galileo-GPS Vertical Guidance, *Proc. of the Institute of Navigation National Technical Meeting*, San Diego, CA, 22-24 Jan 2007.

12. Euler, H.J., and Goad, C.C., 1991. On optimal Filtering of GPS Dual-Frequency Observations without Using Orbit Information. *Bulletin Géodésique,* **65**, 130-143.

13. Gelb, A., 1974. *Applied Optimal Estimation*. Massachusetts Institute of Technology Press, Cambridge, Ma.

14. Hekimoglu, S., and Berber, M., 2003. Effectiveness of robust methods in heterogeneous linear models. *Journal of Geodesy*, **76:** 706–713.

15. Kim, D., and R.B. Langley., 2001. Quality control techniques and issues in GNSS applications: Stochastic modeling and reliability test. *Proc. International Symposium on GNSS/GNSS*, the 8th GNSS Workshop. Jeju Island, Japan, 7-9 Novmeber, 2001.

16. Marsaglia, G., Tsang, W., and Wang, J., 2003. Evaluating Kolmogorov's Distribution. *Journal of Statistical Software*, **8**(18), 1-4.

17. Neri, P., Azoulai, L., and Macabiau, C., 2011. Study of the Temporal Behavior of GPS/GALILEO NSE and RAIM for LPV200. *Proc. of ION GNSS 2011*, Oregon, Portland, 19-23 September 2011.

18. Teunissen, P.J.G., and A.R. Amiri-Simkooei., 2007. Least-squares variance component estimation, *Journal of Geodesy*, **82**(2):65-82, doi:10.1007/s00190-007-0157-x.

19. Teunissen, P. J. G. , and De Bakker P. F., 2012. Single-receiver single-channel multi-frequency GNSS integrity: outliers, slips, and ionospheric disturbances. *Journal of Geodesy*, **87**(2), 161–177.

20. Teunissen, P.J.G., and Kleusberg, A., 1998. *GPS for Geodesy*, 2nd ed., Springer, NY.

21. Teunissen PJG, de Bakker PF (2012) Next Generation GNSS Single Receiver Cycle Slip Reliability, *Proc. VII Hotine-Marussi Symposium on Mathematical Geodesy*, International Association of Geodesy Symposia 137: 159-164

22. Tiberius, C. C. J. M., and Kenselaar, F., 2000. Estimation of the stochastic model for GPS code and phase observables. Surv. Rev., 35(277), 441-454.

23. Tiberius, C., Van Der Marel, H., Sleewaegen, J.M., and Boon F., 2008. Galileo Down to the Millimeter: Analyzing a GIOVE-A/B Double Difference. *Inside GNSS*, **5**: 40-44.

24. Yang, L., Wang, J., Knight, N. L., and Shen, Y., 2013. Outlier separability analysis with a multiple alternative hypotheses test. *Journal of Geodesy*, **87:** 591–604.

25. Yang, L., Knight, N.L., Li, Y., and Rizos, C., 2013. Optimal Fault Detection and Exclusion Applied in GNSS Positioning. *The Journal of Navigation*, **66**(5), 683-700, doi:10.1017/S0373463313000155.

26. Wang, J., C. Satirapod, and C. Rizos., 2002. Stochastic assessment of GNSS carrier phase measurements for precise static relative positioning. *Journal of Geodesy*, **76**(2):95-104, doi:10.1007/s00190-001-0225-6.

27. Ward, P., 1996, GPS Satellite Signal Characteristics, in Understanding GPS Principles and Applications, (ed. Kaplan, E.D.), Artech House Publishers, 83-117.